Monitoring terrestrial water storage, drought and seasonal changes in central Oklahoma with ambient seismic noise

Shuo Zhang[1], Bingxu Luo[2], Yehuda Ben-Zion[3], David E Lumley[1], and Hejun Zhu[1]

[1]University of Texas at Dallas
[2]The University of Texas at Dallas
[3]University of Southern California

March 1, 2023

Abstract

Significant imbalances in terrestrial water storage (TWS) and severe drought have been observed around the world as a consequence of climate changes. Improving our ability to monitor TWS and drought is critical for water-resource management and water-deficit estimation. We use continuous seismic ambient noise to monitor temporal evolution of near-surface seismic velocity, dv/v, in central Oklahoma from 2013 to 2022. The derived dv/v is found to be negatively correlated with gravitational measurements and groundwater depths, showing the impact of groundwater storage on seismic velocities. Seasonal cycling of dv/v follows atmospheric temperature changes with a phase shift, which can be explained by thermo-elastic strain in the uppermost crust and sedimentary cover. The occurrences of droughts appear simultaneously with the local peaks of dv/v, demonstrating the sensitivity of near-surface seismic velocities to droughts. The results illustrate the potential of using seismic data for monitoring TWS and drought at regional to local scales.

Monitoring terrestrial water storage, drought and seasonal changes in central Oklahoma with ambient seismic noise

Shuo Zhang[1], Bingxu Luo[1], Yehuda Ben-Zion[2], David E. Lumley[1,3],Hejun Zhu[1,3]

[1]Department of Geosciences, The University of Texas at Dallas
[2]Department of Earth Science and Southern California Earthquake Center, University of Southern California
[3]Department of Physics, The University of Texas at Dallas

Key Points:

- A long-term trend of dv/v in Oklahoma correlates well with gravity measurement, which may reflect groundwater recharge and discharge.
- Short-term peaks of dv/v agree with the drought index, demonstrating a potential for monitoring meteorological droughts.
- A seasonal cycle of dv/v in central Oklahoma can be explained by thermo-elastic strain driven by atmospheric temperature changes.

Corresponding author: Hejun Zhu, `hejun.zhu@utdallas.edu`

Abstract

Significant imbalances in terrestrial water storage (TWS) and severe drought have been observed around the world as a consequence of climate changes. Improving our ability to monitor TWS and drought is critical for water-resource management and water-deficit estimation. We use continuous seismic ambient noise to monitor temporal evolution of near-surface seismic velocity, dv/v, in central Oklahoma from 2013 to 2022. The derived dv/v is found to be negatively correlated with gravitational measurements and groundwater depths, showing the impact of groundwater storage on seismic velocities. Seasonal cycling of dv/v follows atmospheric temperature changes with a phase shift, which can be explained by thermo-elastic strain in the uppermost crust and sedimentary cover. The occurrences of droughts appear simultaneously with the local peaks of dv/v, demonstrating the sensitivity of near-surface seismic velocities to droughts. The results illustrate the potential of using seismic data for monitoring TWS and drought at regional to local scales.

Plain Language Summary

Terrestrial water storage (TWS) is fundamental to the well-being of inhabitants on Earth. However, current approaches to measure TWS variations have limited temporal or spatial resolution. In this study, we use near-surface seismic velocity variations, dv/v, derived from continuous seismic recordings to monitor changes of TWS in central Oklahoma. A negative correlation between the long-term trend of dv/v with gravity measurements reflects the impact of groundwater recharge/discharge on near-surface seismic velocity. In addition, a seasonal cycling of dv/v has similar periodicity to recordings of air temperature, which can be explained by thermo-elastic strain at the subsurface. Comparisons between dv/v and drought index further show the possibility of using near-surface seismic velocity as a proxy for monitoring severe drought for local communities. Considering the high temporal sampling and flexible spatial deployment, seismometers may be used to monitor subsurface water distributions. This can be useful for sustainable water management and reliable water-deficit estimation.

1 Introduction

Terrestrial water storage (TWS), which mainly includes groundwater, surface water, soil moisture, snow and ice accumulation plays important roles in many studies including the Earth's hydrological cycle (Oki & Kanae, 2006; Famiglietti et al., 2011), climate change (Rodell et al., 2018; Pokhrel et al., 2021), sea-level (Konikow, 2011; J. Reager et al., 2016), drought (Rodell et al., 2009) and flooding (J. T. Reager et al., 2014). The groundwater and surface water are dominant prerequisites for agricultural irrigation, and have important social- and economical-impacts to modern society (Rodell et al., 2009; Famiglietti et al., 2011; Scanlon et al., 2012). Severe climate changes have also led to frequent occurrences of drought and flooding. In addition, increasing demands on water resources for economical and social developments have imposed tremendous stresses on TWS (Feng et al., 2013; Long et al., 2013). Hence, it is critical to accurately and timely monitor the change of TWS in order to maintain sustainable water-resources management and rational water-inadequacy estimation (Alsdorf & Lettenmaier, 2003).

Direct measurements of TWS, such as installing gauges in wells, can accurately assess the levels of aquifers. However, due to the expense of well drilling and instrument maintenance, a limited number of wells typically lead to TWS estimates with a low spatial resolution (Alsdorf & Lettenmaier, 2003). In contrast, remote sensing techniques, such as Global Positioning System (GPS) and Interferometric Synthetic Aperture Radar (InSAR), allow measuring the deformation of the Earth's surface, which can then be used to infer groundwater variations and underground fluid migration (Bawden et al., 2001; Argus et al., 2005). In spite of the high temporal resolution of GPS measurements (K. H. Ji & Herring, 2012), its point-sampling characteristics fail to accurately map lateral heterogeneity of TWS. On the other hand, radar and InSAR can be used to delineate surface deformation with a much higher spatial resolution (Watson et al., 2002; Lanari et al., 2004), but they typically suffer from comparatively low temporal resolution, which depends on the orbital frequency of satellites. Since 2003, the Gravity Recovery and Climate Experiment (GRACE), a joint mission supported by the National Aeronautics and Space Administration (NASA) and the German Aerospace Center, provides detailed information on gravity variations on the Earth's surface by measuring the position changes of twin satellites (Tapley, Bettadpur, Watkins, & Reigber, 2004). These temporal mass changes near the Earth's surface primarily result from near-surface water circulation and migration. As a state-of-the-art technique, GRACE measurements have been widely used to assess TWS variations from regional to global scales (Rodell et al., 2007; Tian et al., 2017), and also enable estimating ice sheet and glacier melting in Greenland and Antarctica (Velicogna & Wahr, 2006a, 2006b; Harig & Simons, 2012). However, its limited temporal sampling (one month) and spatial resolution (around 300−400 km) (Tapley, Bettadpur, Watkins, & Reigber, 2004) cannot satisfy the urgent requirement of managing sustainable water-resource at regional to local scales.

There have been many applications for time-lapse seismic velocity analysis of water injection (Landrø, 2001; Nakata et al., 2022), reservoir monitoring (Rickett & Lumley, 2001; Angerer et al., 2002), and carbon capture and storage (D. Lumley, 2010; Zhu et al., 2019). Because of data availability and computational cost, these classical approaches to monitor temporal changes of the seismic velocities is limited by the occurrence of earthquakes in small regions, which commonly leads to sparse temporal sampling (D. E. Lumley, 2001; Kamei & Lumley, 2017). Over the past decades, continuously recorded seismic ambient noise has been widely used to delineate spatial and temporal variations of seismic velocities within the Earth's crust and upper mantle. It alleviates the restriction of using ballistic wave propagation between earthquakes and seismometers (Campillo & Paul, 2003; Shapiro et al., 2005; Lin et al., 2008; Yao & Van Der Hilst, 2009; Ritzwoller et al., 2011), thus enabling us to image Earth's structure for tectonically inactive regions. Under the assumption of a homogeneous and equal-potential stress field in the study region, the Green's function in a seismic diffusive wavefield can be extracted by cross-correlating recordings between pairs of stations (Claerbout, 1968; Lobkis & Weaver, 2001; Wapenaar & Fokkema, 2006; Snieder, 2006). Seismologists have also used cross- and auto-correlation of different parts of ambient noise and earthquake waveforms to monitor temporal variations of seismic velocities near the Earth's surface. As examples, co- and post-seismic damage and healing processes were studied by measuring seismic velocity changes before and after large earthquakes in California (Brenguier, Campillo, et al., 2008; Taira et al., 2015; Lu & Ben-Zion, 2022), Sichuan (Liu et al., 2014; Pei et al., 2019), Tohoku area (Rubinstein et al., 2007; Minato et al., 2012; Brenguier et al., 2014), and Turkey (Peng & Ben-Zion, 2006). Some studies also demonstrated the potential of using seismic ambient noise to study environmental changes, such as investigating correlations between near-surface seismic velocity changes with precipitation (H. F. Wang, 2017; Q. Wang et al., 2017), temperature changes (Hillers & Ben-Zion, 2011; Wu et al., 2020), freeze-thaw of permafrost (James et al., 2017; Mordret et al., 2016), periodic ocean tide (Ardhuin et al., 2011), and wind speeds (Young et al., 1994). Recently, several studies have successfully utilized ambient noise recordings to monitor crustal velocity changes in response to severe droughts in California (Clements & Denolle, 2018; Mao et al., 2022), Texas (Kim & Lekic, 2019), as well as decadal hydrological and temperature changes in southern Germany (Lecocq et al., 2017).

Since 2008, central Oklahoma has experienced a significant increase in seismicity, some of which led to infrastructure destruction, such as the 2011 Mw 5.7 Prague earthquake (Sun & Hartzell, 2014; Sumy et al., 2017) and the 2016 Mw 5.8 Pawnee earthquake (Barbour et al., 2017; Chen et al., 2017). In response to these events, the United States Geological Survey (USGS) and Oklahoma Geological Survey (OGS) have deployed dense seismic networks to monitor earthquake activity and examine their relation with industry operations, such as saltwater injection during unconventional shale gas production (Keranen et al., 2013; McGarr, 2014; Yeck et al., 2017). These large amounts of continuous seismic recordings provide an important opportunity to investigate environmental changes via seismic ambient noise, and in particular to monitor variations of TWS and droughts in central Oklahoma. Two major bedrock aquifers in central Oklahoma are the Garber-Wellington (GW) in the south and the Vamoosa-Ada (VA) in the east (Figure 1A). Several minor reservoirs, such as the Enid Isolated Terrace (EIT), Cimarron River (Ci), and North Canadian River (NC) also contribute to the hydrological complexity in the study region (Osborn & Hardy, 1999). As an agricultural state, irrigation in Oklahoma highly depends on the supply of groundwater. Detected by the U.S. Drought Monitor (Svoboda et al., 2002), central Oklahoma has suffered from severe droughts in the last decade (Kuwayama et al., 2019). The U.S. is the world's third-largest wheat exporter, and severe droughts in these two major wheat-producing states, Kansas and Oklahoma, led to 7-8% reduction of wheat in 2021 in comparison to their five-year average (Hegarty, 2022). Improving the capability to better monitor water storage in Oklahoma can contribute to sustainable water resources management and steady global food supplys.

2 Data and Methods

Our study area ranges from $97.90°W$ to $96.30°W$ in longitude and $35.20°N$ to $36.50°N$ in latitude (Figure 1A). Nine-year-long (from 2013 to 2022) continuous seismic recordings for all available seismometers are collected as the dataset for this study. Due to the limited number of permanent seismometers deployed in Oklahoma, we also use temporary stations with duration longer than two years to compensate for the data availability. In total, 54 seismometers, mainly from networks NX, OK, GS and O2, are used in Figure 1A. We set 15 and 100 km as the minimum and maximum for the inter-station distance when grouping station pairs and making time-lapse measurements.

Only vertical components of the broadband seismic recordings are used in the analysis. Due to the imbalanced sampling (data only observed at the Earth's surface) and high susceptibility of shallow structures to failure, large shallow velocity changes can be erroneously mapped to smaller variations at greater depths (Juarez & Ben-Zion, 2020). Here, we estimate the depth sensitivity of our measurements based on fundamental mode Rayleigh waves dispersion with a 1-D velocity profile provided by the OGS (Figure S2 in the Supporting Information). In order to monitor groundwater storage near the Earth's surface, we filter the continuous recordings from 0.1 to 1.0 Hz, allowing us to map time-lapse velocity changes down to 1.0 km depth. Our data preprocessing procedures include re-sampling, bandpass-filtering, spectral whitening, instrument response deconvolution, and one-bit normalization (Bensen et al., 2007). The continuous recordings, after preprocessing, are cut into one-hour-long segments. For each station pair, the data segments with the same timestamp are cross-correlated and stacked to construct daily cross-correlation functions (CCFs). Here, we choose a 60-day stacking window with 30-day overlap, which gives us the best performance and stability. The reference CCF for each station pair is the stacked result of all available daily CCFs, while for all daily and refernce CCFs, the positive and negative branches are stacked to boost the signal-to-noise ratio. Once we gather the daily and reference CCFs, their relative time shift, dt, can be computed by using the Moving Window Cross Spectrum method (MWCS) (Clarke et al., 2011), during which the surface and coda waves are isolated by applying dynamic time windows with apparent velocities of 3.0 and 2.0 km/s, respectively (Figure S3 in Supprting Information). With the assumption of homogeneous velocity perturbation, the relative time delay (dt/t) between the daily and reference CCFs should be negatively proportional to the velocity variation (dv/v), i.e., dv/v=-dt/t (Poupinet et al., 1984). More detailed information on the post-processing procedure of ambient noise CCFs can be found in Section S2 of the Supporting Information.

The used dv/v measurements have acceptable uncertainties with respect to frequencies and azimuthal angles. With the same dataset and workflow, four different frequency bands (0.1-1.0 Hz, 0.5-2.0 Hz, 0.2-0.8 Hz, 0.4-1.6 Hz) give us similar dv/v patterns, especially for recovering seasonal variations and long-term trends (Figure S6 in the Supporting Information). The CCFs may also be affected by the heterogeneous distributions of noise sources, such as periodic ocean tides (Ardhuin et al., 2011) and wind speeds (Young et al., 1994). Here, we group the station pairs and re-calculate dv/v according to their azimuthal angles and the similarity among four azimuth groups ($0-90°$, $90-180°$, $180-270°$, $270-360°$) suggests that the measured dv/v mainly reflect near-surface seismic velocity variations in the study area, rather than heterogeneous noise source distributions (Figure S7 in the Supporting Information). More details about the uncertainty estimation can be found in Section S3 of the Supporting Information.

3 Results

3.1 Seasonal changes and long-term trends

We compute the mean and median of dv/v among all station pairs in order to illustrate the averaged temporal evolution of near-surface seismic velocity in central Oklahoma (Figure 1B). The raw dv/v time series are smoothed by a Gaussian filter with standard deviation σ=6 days, in order to eliminate unrealistic high-frequency fluctuations. The uncertainty of dv/v is comparatively small, within 5% for most measurements (blue shade in Figure 1B). Some temporary stations were not working, resulting in relatively larger uncertainty from 2016 to 2018. Since 2014, dv/v reduces gradually until the middle of 2017 and then rebounds to its peak value (+0.03%) around the end of 2018 (Figure 1B). After that, it declines further to -0.02% until 2020, and then fluctuates in a relatively low-value zone. Besides this long-term fluctuation, we also observe clear seasonal cycling in dv/v measurements. Statistically stacking the intra-annual pattern of each year, we find that dv/v declines annually to a trough during the summer time (April to June), whereas its peak value commonly appears in the winter season from October to December (Figure 1D). Both seasonal and long-term changes can be clearly identified in the time-frequency analysis of the dv/v measurements by using moving window Fourier transform (Figure 1C). A continuous response, centering around one year period, reflects the seasonal cycling, while another strong response existing at periods greater than two years represents the long-term trend in our measurements.

3.2 Comparison with GRACE observations

Figure 2 compares the dv/v results with the GRACE measurements (Syed et al., 2008; Landerer & Swenson, 2012; Richard Peltier et al., 2018), expressed in terms of water equivalent thickness in centimeters. The gap in the GRACE measurements around 2018 comes from an observational gap between the GRACE and GRACE-FO missions, with the latter launched in May 2018. The sampling rates for both GRACE and GRACE-FO missions are one month. To compare signals, both dv/v and GRACE data are interpolated and filtered into the same frequency band. We further quantify the similarity between GRACE and dv/v results by applying a moving window cross-correlation, with a 800-day-long sliding window, between these two time-series (Figure 2B).

Overall, the GRACE data is negatively correlated with our dv/v results, and the absolute cross-correlation coefficient in Figure 2B is greater than 0.7 with almost zero time lag, suggesting that gravity perturbations and seismic velocity variations reflect similar environmental changes in central Oklahoma. Furthermore, we use a least-square regression to determine a linear relation between dv/v and GRACE results (Δh), which gives $dv/v = -1.68\times10^{-3}\Delta h - 9.61\times10^{-3}$, with the final data misfit as 0.00848. The confidential ellipse with 2σ (black dashed ellipse in Figure 2C) covers most data points, suggesting a good linear fitting between these two independent datasets. In comparison to the annual statistical stacking of dv/v shown in Figure 1D, we also observe seasonal cycling in the GRACE data, but with an opposite intra-annual pattern (Figure 2D). The strong annual similarity between these two independent time series again suggests that they may reflect similar physical processes, such as variations of TWS near the Earth's surface (Tapley, Bettadpur, Ries, et al., 2004; Rodell et al., 2007; Famiglietti et al., 2011).

As a state-of-the-art tool for monitoring TWS (Rodell et al., 2018), the limited spatial resolution (300 to 400 km) and temporal sampling (one month) of the GRACE measurements cannot satisfy current requirements of ground and surface water storage management at regional to local scales. In contrast, seismic ambient noise measurements have the considerably higher temporal and spatial resolution, depending on the specific deployment configuration, and can be used to monitor the intra-seasonal persistence of TWS deficits and surpluses in a relatively small basin with near real-time fashion and low costs. Furthermore, since more than 13,000 permanent seismometers have already been deployed around the world and can be openly accessed through the Data Management Center of the Incorporated Research Institutions for Seismology (IRIS-DMC), continuous seismic noise recordings provide a compelling supplement to the GRACE measurements for monitoring water balance on the Earth's surface.

3.3 Correlation with groundwater measurements

As a low-latitude inland state, surface water storage and snowfall are negligible in Oklahoma (Swenson et al., 2008), so groundwater storage and soil moisture are the major contributors to the TWS in Oklahoma. Negative correlations between groundwater levels and dv/v have been observed in California (Clements & Denolle, 2018; Mao et al., 2022; Qin et al., 2022) and Germany (Lecocq et al., 2017). Also, the spatiotemporal variations of seismic velocity, after projecting into 2-D maps by using coda wave sensitivity kernels (Mao et al., 2022), are coherent with the discharge and recharge of aquifers in California. The sensitivity of near-surface seismic velocity to groundwater storage can be directly examined by comparing dv/v with groundwater levels.

Deployed by the OGS, the gauge in the Spencer well measures groundwater depths for monitoring the status of the Garber-Wellington (GW) aquifer (Mashburn et al., 2014), which can be obtained from the Oklahoma Water Resource Board (OWRB). Considering lateral variations of seismic velocities, a local dv/v is measured from three seismometers (OK.CHOK, OK.SMO, OK.SWND) surrounding the Spencer well by using the workflow described in Section 2. Starting at 15.5 ft in 2016 (Figure 3A), a monotonic increase of the groundwater depth, indicating a discharge of the GW aquifer, is well correlated with the dynamic increase of seismic velocity around the Spencer well. In contrast, the groundwater level gradually reduces from 17.0 ft in 2019 to 15.0 ft in 2022, representing the recharge of GW aquifer, while the seismic velocity correspondingly decreases by about 0.06 % during the same period (Figure 3A). Similar to the gravitational variations shown in Figure 2A, this negative correlation between groundwater levels and long-term trend of local dv/v further illustrates the sensitivity of near-surface seismic velocities to groundwater recharge/discharge, and demonstrates the capability of using seismic data to monitor TWS with higher temporal and spatial resolution. The seasonal variations around the long-term changes are modeled in terms of thermo-elastic strain (Figure 3B-D) and discussed in Section 4.

3.4 Comparison with precipitation and drought index

Next, we compare the dv/v measurements with recordings from precipitation and drought monitoring. Figure 4A shows the history of drought index in central Oklahoma, collected from the USDM (Noel et al., 2020), which classifies the drought condition in five levels, D0 to D4, representing abnormal, moderate, severe, extreme, and exceptional droughts, respectively. From the USDM recordings for central Oklahoma, up to 80% of areas suffered from different levels of drought (D1–D4) from January 2014 to April 2015. Another two severe droughts appeared from November 2016 to May 2017 and December 2017 to October 2018, when 60% of areas in central Oklahoma were under moderate drought (D1) and up to 20% of areas were exceptionally dry (D4).

The drought index is negatively correlated with the precipitation data (Figure 4B) collected from the Oklahoma Climatological Survey (Boone et al., 2012). For instance, no drought is observed in May 2015 and April 2019 when there were high precipitation volumes (greater than +10 inches precipitation anomaly). In contrast, due to comparatively less precipitation in April 2014 (-10 inches precipitation anomaly), 40% of areas in central Oklahoma were in D4-level drought. Comparably, the dv/v results decrease since February 2014 and reach a minimum in March 2016 when the drought in central Oklahoma is less severe, while they increases during the next severe drought until January 2018 when 90% of areas were in D2-level drought. Because of the frequent and heavy rains in 2019, dv/v fluctuates in a relatively low-value zone where only abnormal droughts were detected in central Oklahoma. It is interesting to note that in central Oklahoma, almost every major drought season coincides with a rapid increase of dv/v. These correlations among the drought index, precipitation, and dv/v again illustrate that near-surface seismic velocities are influenced by climate changes.

4 Discussion

4.1 Potential impact of pore pressure on seismic velocity changes

Seismic velocities within the Earth's uppermost crust may be affected by a variety of factors, including environmental changes (Hillers et al., 2015; Lecocq et al., 2017; Clements & Denolle, 2018; Mao et al., 2022), earthquakes (Peng & Ben-Zion, 2006; Brenguier, Campillo, et al., 2008; Bonilla et al., 2019; Qiu et al., 2020), and volcanic activities (Sens-Schönfelder & Wegler, 2006; Brenguier, Shapiro, et al., 2008; Brenguier et al., 2014, 2016). Multiple factors can lead to changes in effective confining pressure or dynamic stresses, and eventually result in seismic velocity perturbations with different magnitudes and characteristic time scales. For instance, tides, temperature changes, snow loading, or sea level changes typically produce 10^{-5} to 10^{-3} velocity changes with time scales ranging from hours to years (Yamamura et al., 2003; Taira et al., 2018), whereas tectonic/volcanic activities might also lead to 0.1% to more than 10% velocity perturbations (Niu et al., 2008; Brenguier et al., 2014; Pei et al., 2019). Here, it is important to note that the absolute amplitude of derived dv/v depends on the temporal sampling rate used in the analysis (Bonilla et al., 2019). Longer time windows reflect averages over larger time scales and spatial extent, and result in smaller amplitudes than local changes that may be resolved by very short time windows.

Seismic velocity is known to be sensitive to decreasing/increasing effective confining pressure, which affect opening/closure of the microcracks and/or pore space during recharge/discharge of water storage (Birch, 1960; Simmons, 1964; Nur & Simmons, 1969). As we can monitor in-situ seismic velocity variations, a corresponding sensitivity allows estimating changes of effective confining pressure that is relative to water storage in Oklahoma. Here we attempt to calculate the potential stress sensitivity based on the linear regression between dv/v and GRACE measurements (Figure 2C). Since the GRACE measurement is expressed as equivalent water thickness in centimeters (Δh), the slope value connecting gravity and dv/v ($-1.68\times10^{-3} cm^{-1}$) can be transfered to the potential stress sensitivity of dv/v by $\Delta P = \rho g \Delta h$. Converting all variables into standard units, the estimated stress sensitivity is -1.72×10^{-7} Pa^{-1}, which is in the same magnitude as the in-situ measurements of previous studies, 10^{-7}Pa^{-1} (Yamamura et al., 2003; Silver et al., 2007). This linear slope also allows estimating, in future studies, the changes of gravity for areas that are too small to be sampled by the GRACE mission. In addition, it provides a possibility to estimate regional stress perturbation from measurements for relative seismic velocity changes.

The clear correlations between our dv/v results with GRACE (Figure 2) and groundwater well measurements (Figure 3A) suggests that when the pore space of sedimentary rocks is filled with water during aquifer recharge, the increasing pore-pressure, and related decreasing effective confining pressure and rock rigidity, generates the reduction of near-surface seismic velocity (Dong & Lu, 2016; Qin et al., 2022). In contrast, the increasing confining pressure and rigidity during drought periods lead to increases in seismic velocity. This helps to explain the correspondence between severe droughts with local peaks in the derived dv/v results shown in Figure 4A.

4.2 Potential impact of rock density changes on near-surface seismic velocity

Besides pore pressure changes, bulk density changes may also lead to seismic velocity perturbations. It has been concluded that the bulk density ρ, comparing with shear modulus G, may play a more significant role on shear velocity, with respect to water saturation (Nur & Simmons, 1969; M. Wyllie et al., 1962; Mavko & Jizba, 1991). It has recently been validated in a laboratory experiment (Li et al., 2018) that increasing water saturation, from 0 to about 100%, leads to a larger decay in shear velocity than shear modulus solely. We, therefore, discuss the potential impact of density changes on seismic velocity to interpret our results.

To quantitatively investigate the influence of bulk density, we introduce a two-layer conceptual model, with a dry upper layer and a water-saturated lower layer, to represent the aquifer contact. Taking the thicknesses of the dry upper layer and the water table as L_1 and L_2, respectively, the apparent velocity of this two-layer model can be computed by using the following Voigt-Reuss-Hill approximation (M. R. J. Wyllie et al., 1956; Mavko et al., 2020),

$$V_{app} = \frac{L_1}{L_1 + L_2} V_1 + \frac{L_2}{L_1 + L_2} V_2 \quad , \tag{1}$$

where V_1 and V_2 stand for the velocities of the upper and lower layers. We assume a homogeneous and isotropic medium in each layer, $V_s = \sqrt{G/\rho}$ (Mavko et al., 2020), and a constant shear modulus G that is unchanged by water saturation for simplicity (Nur & Simmons, 1969; M. Wyllie et al., 1962). With the definition of dry and saturated rocks (Gassmann, 1951), the apparent shear velocity of this two-layer model can be re-written as:

$$\begin{aligned} V_{s,app} &= \frac{L_1}{L_1 + L_2}\sqrt{\frac{G}{\rho_{dry}}} + \frac{L_2}{L_1 + L_2}\sqrt{\frac{G}{\rho_{sat}}} \quad , \\ &= \frac{L_1}{L_1 + L_2}\sqrt{\frac{G}{(1-\phi)\rho_0}} + \frac{L_2}{L_1 + L_2}\sqrt{\frac{G}{(1-\phi)\rho_0 + \phi\rho_w}} \quad . \end{aligned} \tag{2}$$

where ρ_{dry} and ρ_{sat}, controlled by the porosity ϕ, denote the averaged densities of dry and fully saturated rocks, and ρ_0 and ρ_w represent the densities of host rock and pure water, respectively.

To represent the circumstance in Oklahoma, we use $G = 24.0\ GPa$, $\phi = 0.3$, and $\rho_0 = 2.65\ g/cm^3$ (D. C. Wyllie & Mah, 2004) to approximate the sediment, with $\rho_w = 1.00\ g/cm^3$. The total thickness of the two-layer model is $L = L_1+L_2 = 100\ m$, which is equivalent to the average thickness of the GW aquifer (Mashburn et al., 2014). When the groundwater level L_1 changes from 5 to 6 m representing the discharge of the GW aqufier, the apparent shear velocity $V_{s,app}$ reduces by 2.9 m/s with $dv_s/v_s = -0.03\%$, which is comparable to the measured dv/v ($\pm 0.04\%$) from seismic ambient noise recordings (Figure 1B). In spite of the simplification of the model, this synthetic velocity perturbation analysis provides a negative correlation between time-lapse seismic velocity changes and groundwater variations through the change of apparent rock density in water reservoirs.

We provide two possible mechanisms, pore-pressure and bulk density, for interpreting the observed negative correlation between groundwater storage and long-term seismic velocity variations. However, at the current stage, we cannot further distinguish these two mechanisms, or assess the non-uniqueness in modeling and inversion, because of limited knowledge of rock properties in Oklahoma, such as averaged porosity around the water reservior, elastic moduli of dry rocks, approximated water saturation in dry and wet seasons, confining pressure around aquifers, etc, which require more detailed investigations in the future.

4.3 Thermo-elastic effects on the seasonal changes of near-surface seismic velocities

Annual atmospheric temperature variations have been used to explain seasonal changes of dv/v in many regions, including California (Meier et al., 2010; Hillers et al., 2015; Qiu et al., 2020; Clements & Denolle, 2023), Kyushu Island (Q. Wang et al., 2017), northern Chile (Richter et al., 2014), and Mars (Qin et al., 2023). The nonlinear relation between air temperature and seismic velocity changes can be modeled in terms of thermoelastic strain at the subsurface (Berger, 1975; Ben-Zion & Leary, 1986; Tsai, 2011). This process has been investigated in laboratory experiments by heating and cooling rock samples (Snieder et al., 2002). Here, we use the following experssions of thermo-elastic strain from Ben-Zion and Leary (1986) and Tsai (2011) to explain the relation between air temperature and seismic velocity in central Oklahoma,

$$
\begin{aligned}
\frac{\mathrm{d}v}{v} &= A(t)e^{-kz}\frac{\lambda+3\mu+m}{\mu}sin(kz)(1-2\nu) \quad , \\
A(t) &= \frac{1+\nu}{1-\nu}k\alpha_{th}T_0\sqrt{\frac{\kappa}{\omega}}e^{-\sqrt{\frac{\omega}{2\kappa}}y_b}cos\left(\omega t-\sqrt{\frac{\omega}{2\kappa}}y_b-\frac{\pi}{4}\right) \quad .
\end{aligned}
\tag{3}
$$

Here T_0 and ω denote the mean value and frequency of the temperature record, α_{th} and κ are the linear thermo-expansion coefficient and thermo-diffusivity, respectively, λ and μ are two Lamé parameters, and ν stands for the Poisson's ratio. The values of these model parameters for the study region are collected from previous studies (Deming & Borel, 1995; S. Ji et al., 2010; Zhai et al., 2019), and are listed in Figure 3C. The parameter m in Equation 3 represents the second Murnaghan elastic constant, while y_b represents the thickness of an unconsolidated cover layer. To simulate velocity variations induced by temperature changes, we determine y_b and m by searching for the minimum misfit between observed dv/v and simulated dv/v from Equation 3. This grid-search (Figure 3D) gives values of $y_b = 2.89\ m$ and $m = -1.78 \times 10^7 GPa$, which are reasonable approximations for central Oklahoma.

As shown in Figure 3B, the time series of the simulated (green) and measured (blue) dv/v have good correspondence in both amplitudes and phases with a cross-correlation coefficient of 0.843. In addition, the averaged temporal shift between the measured dv/v and temperature fluctuations (red) is around 63 days. The similarity between the simulated and observed seasonal variations of dv/v suggests that air temperature changes are another important environmental factor affecting changes of near-surface seismic velocity. A mismatch between the observed and thermo-elastic simulated dv/v is observed from 2016 to 2019, where the time shift ranges from 54 days in 2016 to 12 days in 2019. Potential causes of these local deviations include changes in the effective layer thickness y_b resulting from soil moisture variations, and larger uncertainty due to reduced data coverage associated with fewer temporary seismometers during this period (Section 2).

5 Conclusions

Taking advantage of recently deployed seismometers in central Oklahoma, we estimate relative seismic velocity variations (dv/v) using continuous ambient seismic noise recordings. The negative correlation between dv/v and GRACE measurements, as well as groundwater levels, can be explained by changes of near-surface seismic velocities due to changes of pore pressure and/or bulk density induced by water saturation. The time delay between the seasonal cycling of dv/v and air temperature recordings can be explained in terms of thermo-elastic strain at the subsurface. The simultaneous occurrences of severe droughts and local peaks of dv/v in central Oklahoma illustrate the sensitivity of near-surface seismic velocities to meteorological droughts. Considering the high temporal sampling rates and flexible spatial resolution of seismic recordings, using analyses of the type performed in this paper can improve the ability to monitor terrestrial water distribution, which is critical for sustainable water-resource management and accurate water-deficit estimation.

Acknowledgments

The study was supported by the National Science Foundation (Grant EAR-2042098), the U.S. Department of Energy Office of Science (Award DE-SC0016520), and the Geophysical Consortium at the University of Texas at Dallas. The raw continuous seismic recordings are collected and pre-processed by using Obspy. We use the MSNoise package to measure temporal evolution of near-surface seismic velocity from ambient noise recordings. The groundwater data are collected from the Oklahoma Geological Survey and the Oklahoma Geological Water Resource (`https://www.owrb.ok.gov/maps/PMG/owrbdata_GW.html`). The historical precipitation recordings for central Oklahoma are accessed from the Oklahoma Climatological Board (`https://www.mesonet.org/index.php/weather/monthly_rainfall_table`). The historical air temperature recordings in Oklahoma are downloaded from Weather Underground (`www.wunderground.com/history`). The Colorado Center of Astrodynamics Research compiled the GRACE and GRACE-FO gravitational data (`https://ccar.colorado.edu/grace/gsfc.html`). The National Drought Mitigation Center at the University of Nebraska-Lincoln provided the historical drought index for central Oklahoma (`https://droughtmonitor.unl.edu/DmData/DataDownload/DSCI.aspx`).

References

Alsdorf, D. E., & Lettenmaier, D. P. (2003). Tracking fresh water from space. *Science*, *301*(5639), 1491–1494.

Angerer, E., Crampin, S., Li, X.-Y., & Davis, T. L. (2002). Processing, modelling and predicting time-lapse effects of overpressured fluid-injection in a fractured reservoir. *Geophysical Journal International*, *149*(2), 267–280.

Ardhuin, F., Stutzmann, E., Schimmel, M., & Mangeney, A. (2011). Ocean wave sources of seismic noise. *Journal of Geophysical Research: Oceans*, *116*(C9).

Argus, D. F., Heflin, M. B., Peltzer, G., Crampé, F., & Webb, F. H. (2005). Interseismic strain accumulation and anthropogenic motion in metropolitan los angeles. *Journal of Geophysical Research: Solid Earth*, *110*(B4).

Barbour, A. J., Norbeck, J. H., & Rubinstein, J. L. (2017). The effects of varying injection rates in osage county, oklahoma, on the 2016 m w 5.8 pawnee earthquake. *Seismological Research Letters*, *88*(4), 1040–1053.

Bawden, G. W., Thatcher, W., Stein, R. S., Hudnut, K. W., & Peltzer, G. (2001). Tectonic contraction across los angeles after removal of groundwater pumping effects. *Nature*, *412*(6849), 812–815.

Bensen, G., Ritzwoller, M., Barmin, M., Levshin, A. L., Lin, F., Moschetti, M., … Yang, Y. (2007). Processing seismic ambient noise data to obtain reliable broad-band surface wave dispersion measurements. *Geophysical journal international*, *169*(3), 1239–1260.

Ben-Zion, Y., & Leary, P. (1986). Thermoelastic strain in a half-space covered by unconsolidated material. *Bulletin of the Seismological Society of America*, *76*(5), 1447–1460.

Berger, J. (1975). A note on thermoelastic strains and tilts. *Journal of Geophysical Research*, *80*(2), 274–277.

Birch, F. (1960). The velocity of compressional waves in rocks to 10 kilobars: 1. *Journal of Geophysical Research*, *65*(4), 1083–1102.

Bonilla, L. F., Guéguen, P., & Ben-Zion, Y. (2019). Monitoring coseismic temporal changes of shallow material during strong ground motion with interferometry and autocorrelationmonitoring coseismic temporal changes of shallow material during strong ground motion. *Bulletin of the Seismological Society of America*, *109*(1), 187–198.

Boone, K. M., McPherson, R. A., Richman, M. B., & Karoly, D. J. (2012). Spatial coherence of rainfall variations using the oklahoma mesonet. *International journal of climatology*, *32*(6), 843–853.

Brenguier, F., Campillo, M., Hadziioannou, C., Shapiro, N. M., Nadeau, R. M., & Larose, É. (2008). Postseismic relaxation along the san andreas fault at parkfield from continuous seismological observations. *science*, *321*(5895), 1478–1481.

Brenguier, F., Campillo, M., Takeda, T., Aoki, Y., Shapiro, N., Briand, X., ... Miyake, H. (2014). Mapping pressurized volcanic fluids from induced crustal seismic velocity drops. *Science*, *345*(6192), 80–82.

Brenguier, F., Rivet, D., Obermann, A., Nakata, N., Boué, P., Lecocq, T., ... Shapiro, N. (2016). 4-d noise-based seismology at volcanoes: Ongoing efforts and perspectives. *Journal of Volcanology and Geothermal Research*, *321*, 182–195.

Brenguier, F., Shapiro, N. M., Campillo, M., Ferrazzini, V., Duputel, Z., Coutant, O., & Nercessian, A. (2008). Towards forecasting volcanic eruptions using seismic noise. *Nature Geoscience*, *1*(2), 126–130.

Campillo, M., & Paul, A. (2003). Long-range correlations in the diffuse seismic coda. *Science*, *299*(5606), 547–549.

Chen, X., Nakata, N., Pennington, C., Haffener, J., Chang, J. C., He, X., ... Walter, J. I. (2017). The pawnee earthquake as a result of the interplay among injection, faults and foreshocks. *Scientific Reports*, *7*(1), 1–18.

Claerbout, J. F. (1968). Synthesis of a layered medium from its acoustic transmission response. *Geophysics*, *33*(2), 264–269.

Clarke, D., Zaccarelli, L., Shapiro, N., & Brenguier, F. (2011). Assessment of resolution and accuracy of the moving window cross spectral technique for monitoring crustal temporal variations using ambient seismic noise. *Geophysical Journal International*, *186*(2), 867–882.

Clements, T., & Denolle, M. A. (2018). Tracking groundwater levels using the ambient seismic field. *Geophysical Research Letters*, *45*(13), 6459–6465.

Clements, T., & Denolle, M. A. (2023). The seismic signature of california's earthquakes, droughts, and floods. *Journal of Geophysical Research: Solid Earth*, *128*(1), e2022JB025553. doi: https://doi.org/10.1029/2022JB025553

Deming, D., & Borel, R. A. (1995). Evidence for climatic warming in northcentral oklahoma from analysis of borehole temperatures. *Journal of Geophysical Research: Solid Earth*, *100*(B11), 22017–22032.

Dong, Y., & Lu, N. (2016). Dependencies of shear wave velocity and shear modulus of soil on saturation. *Journal of Engineering Mechanics*, *142*(11), 04016083.

Famiglietti, J. S., Lo, M., Ho, S. L., Bethune, J., Anderson, K., Syed, T. H., ... Rodell, M. (2011). Satellites measure recent rates of groundwater depletion in california's central valley. *Geophysical Research Letters*, *38*(3).

Feng, W., Zhong, M., Lemoine, J.-M., Biancale, R., Hsu, H.-T., & Xia, J. (2013). Evaluation of groundwater depletion in north china using the gravity recovery and climate experiment (grace) data and ground-based measurements. *Water Resources Research*, *49*(4), 2110–2118.

Gassmann, F. (1951). Elastic waves through a packing of spheres. *GEOPHYSICS*, *16*(4), 673-685. Retrieved from https://doi.org/10.1190/1.1437718 doi: 10.1190/1.1437718

Harig, C., & Simons, F. J. (2012). Mapping greenland's mass loss in space and time. *Proceedings of the National Academy of Sciences*, *109*(49), 19934–19937.

Hegarty, S. (2022). *Satellites give clues about the coming global harvest.* Retrieved July 15, 2022, from https://www.bbc.com/news/world-62149522

Hillers, G., & Ben-Zion, Y. (2011). Seasonal variations of observed noise amplitudes at 2–18 hz in southern california. *Geophysical Journal International*, *184*(2), 860–868.

Hillers, G., Ben-Zion, Y., Campillo, M., & Zigone, D. (2015). Seasonal variations of seismic velocities in the san jacinto fault area observed with ambient seismic noise. *Geophysical Journal International*, *202*(2), 920–932.

James, S., Knox, H., Abbott, R., & Screaton, E. (2017). Improved moving window cross-spectral analysis for resolving large temporal seismic velocity changes in permafrost. *Geophysical Research Letters*, *44*(9), 4018–4026.

Ji, K. H., & Herring, T. A. (2012). Correlation between changes in groundwater levels and surface deformation from gps measurements in the san gabriel valley, california. *Geophysical Research Letters*, *39*(1).

Ji, S., Sun, S., Wang, Q., & Marcotte, D. (2010). Lamé parameters of common rocks in the earth's crust and upper mantle. *Journal of Geophysical Research: Solid*

Earth, *115*(B6).

Juarez, A., & Ben-Zion, Y. (2020). Effects of shallow-velocity reductions on 3d propagation of seismic waves. *Seismological Society of America*, *91*(6), 3313–3322.

Kamei, R., & Lumley, D. (2017). Full waveform inversion of repeating seismic events to estimate time-lapse velocity changes. *Geophysical Journal International*, *209*(2), 1239–1264.

Keranen, K. M., Savage, H. M., Abers, G. A., & Cochran, E. S. (2013). Potentially induced earthquakes in oklahoma, usa: Links between wastewater injection and the 2011 mw 5.7 earthquake sequence. *Geology*, *41*(6), 699–702.

Kim, D., & Lekic, V. (2019). Groundwater variations from autocorrelation and receiver functions. *Geophysical Research Letters*, *46*(23), 13722–13729.

Konikow, L. F. (2011). Contribution of global groundwater depletion since 1900 to sea-level rise. *Geophysical Research Letters*, *38*(17).

Kuwayama, Y., Thompson, A., Bernknopf, R., Zaitchik, B., & Vail, P. (2019). Estimating the impact of drought on agriculture using the us drought monitor. *American Journal of Agricultural Economics*, *101*(1), 193–210.

Lanari, R., Lundgren, P., Manzo, M., & Casu, F. (2004). Satellite radar interferometry time series analysis of surface deformation for los angeles, california. *Geophysical Research Letters*, *31*(23).

Landerer, F. W., & Swenson, S. (2012). Accuracy of scaled grace terrestrial water storage estimates. *Water resources research*, *48*(4).

Landrø, M. (2001). Discrimination between pressure and fluid saturation changes from time-lapse seismic data. *Geophysics*, *66*(3), 836–844.

Lecocq, T., Longuevergne, L., Pedersen, H. A., Brenguier, F., & Stammler, K. (2017). Monitoring ground water storage at mesoscale using seismic noise: 30 years of continuous observation and thermo-elastic and hydrological modeling. *Scientific reports*, *7*(1), 1–16.

Li, D., Wei, J., Di, B., Ding, P., Huang, S., & Shuai, D. (2018). Experimental study and theoretical interpretation of saturation effect on ultrasonic velocity in tight sandstones under different pressure conditions. *Geophysical Journal International*, *212*(3), 2226–2237.

Lin, F.-C., Moschetti, M. P., & Ritzwoller, M. H. (2008). Surface wave tomography of the western united states from ambient seismic noise: Rayleigh and love wave phase velocity maps. *Geophysical Journal International*, *173*(1), 281–298.

Liu, Z., Huang, J., Peng, Z., & Su, J. (2014). Seismic velocity changes in the epicentral region of the 2008 wenchuan earthquake measured from three-component ambient noise correlation techniques. *Geophysical Research Letters*, *41*(1), 37–42.

Lobkis, O. I., & Weaver, R. L. (2001). On the emergence of the green's function in the correlations of a diffuse field. *The Journal of the Acoustical Society of America*, *110*(6), 3011–3017.

Long, D., Scanlon, B. R., Longuevergne, L., Sun, A. Y., Fernando, D. N., & Save, H. (2013). Grace satellite monitoring of large depletion in water storage in response to the 2011 drought in texas. *Geophysical Research Letters*, *40*(13), 3395–3401.

Lu, Y., & Ben-Zion, Y. (2022). Regional seismic velocity changes following the 2019 m w 7.1 ridgecrest, california earthquake from autocorrelations and p/s converted waves. *Geophysical Journal International*, *228*(1), 620–630.

Lumley, D. (2010). 4d seismic monitoring of co 2 sequestration. *The Leading Edge*, *29*(2), 150–155.

Lumley, D. E. (2001). Time-lapse seismic reservoir monitoring. *Geophysics*, *66*(1), 50–53.

Mao, S., Lecointre, A., van der Hilst, R. D., & Campillo, M. (2022). Space-time monitoring of groundwater fluctuations with passive seismic interferometry. *Nature communications*, *13*(1), 1–9.

Marsh, S., & Holland, A. (2016). Comprehensive fault database and interpretive fault map of oklahoma. *Oklahoma Geol. Surv. Open-File Rep. OF2-2016, Oklahoma Geological Survey, Norman, OK*.

Mashburn, S. L., Ryter, D., Neel, C. R., Smith, S. J., & Magers, J. S. (2014). *Hydrogeology and simulation of groundwater flow in the central oklahoma (garber-wellington) aquifer, oklahoma, 1987 to 2009, and simulation of available water in storage, 2010-2059.* US Department of the Interior, US Geological Survey.

Mavko, G., & Jizba, D. (1991). Estimating grain-scale fluid effects on velocity dispersion in rocks. *Geophysics*, *56*(12), 1940–1949.

Mavko, G., Mukerji, T., & Dvorkin, J. (2020). *The rock physics handbook.* Cambridge university press.

McGarr, A. (2014). Maximum magnitude earthquakes induced by fluid injection. *Journal of Geophysical Research: solid earth*, *119*(2), 1008–1019.

Meier, U., Shapiro, N. M., & Brenguier, F. (2010). Detecting seasonal variations in seismic velocities within los angeles basin from correlations of ambient seismic noise. *Geophysical Journal International*, *181*(2), 985–996.

Minato, S., Tsuji, T., Ohmi, S., & Matsuoka, T. (2012). Monitoring seismic velocity change caused by the 2011 tohoku-oki earthquake using ambient noise records. *Geophysical Research Letters*, *39*(9).

Mordret, A., Mikesell, T. D., Harig, C., Lipovsky, B. P., & Prieto, G. A. (2016). Monitoring southwest greenland's ice sheet melt with ambient seismic noise. *Science advances*, *2*(5), e1501538.

Nakata, R., Jang, U.-G., Lumley, D., Mouri, T., Nakatsukasa, M., Takanashi, M., & Kato, A. (2022). Seismic time-lapse monitoring of near-surface microbubble water injection by full waveform inversion. *Geophysical Research Letters*, e2022GL098734.

Niu, F., Silver, P. G., Daley, T. M., Cheng, X., & Majer, E. L. (2008). Preseismic velocity changes observed from active source monitoring at the parkfield safod drill site. *Nature*, *454*(7201), 204–208.

Noel, M., Bathke, D., Fuchs, B., Gutzmer, D., Haigh, T., Hayes, M., … Svoboda, M. (2020). Linking drought impacts to drought severity at the state level. *Bulletin of the American Meteorological Society*, *101*(8), E1312–E1321.

Nur, A., & Simmons, G. (1969). The effect of saturation on velocity in low porosity rocks. *Earth and planetary science letters*, *7*(2), 183–193.

Oki, T., & Kanae, S. (2006). Global hydrological cycles and world water resources. *science*, *313*(5790), 1068–1072.

Osborn, N. I., & Hardy, R. H. (1999). *Statewide groundwater vulnerability map of oklahoma*. Oklahoma Water Resources Board Oklahoma City, OK, USA.

Pei, S., Niu, F., Ben-Zion, Y., Sun, Q., Liu, Y., Xue, X., … Shao, Z. (2019). Seismic velocity reduction and accelerated recovery due to earthquakes on the longmenshan fault. *Nature Geoscience*, *12*(5), 387–392.

Peng, Z., & Ben-Zion, Y. (2006). Temporal changes of shallow seismic velocity around the karadere-düzce branch of the north anatolian fault and strong ground motion. *Pure and Applied Geophysics*, *163*, 567–600.

Pokhrel, Y., Felfelani, F., Satoh, Y., Boulange, J., Burek, P., Gädeke, A., ... others (2021). Global terrestrial water storage and drought severity under climate change. *Nature Climate Change*, *11*(3), 226–233.

Poupinet, G., Ellsworth, W., & Frechet, J. (1984). Monitoring velocity variations in the crust using earthquake doublets: An application to the calaveras fault, california. *Journal of Geophysical Research: Solid Earth*, *89*(B7), 5719–5731.

Qin, L., Qiu, H., Nakata, N., Deng, S., Levander, A., & Ben-Zion, Y. (2023, 12). Variable Daily Autocorrelation Functions of High-Frequency Seismic Data on Mars. *Seismological Research Letters*. doi: 10.1785/0220220196

Qin, L., Steidl, J. H., Qiu, H., Nakata, N., & Ben-Zion, Y. (2022). Monitoring seasonal shear wave velocity changes in the top 6 m at garner valley in southern california with borehole data. *Geophysical Research Letters*, *49*(23), e2022GL101189.

Qiu, H., Hillers, G., & Ben-Zion, Y. (2020). Temporal changes of seismic velocities in the san jacinto fault zone associated with the 2016 m w 5.2 borrego springs earthquake. *Geophysical Journal International*, *220*(3), 1536–1554.

Reager, J., Gardner, A., Famiglietti, J., Wiese, D., Eicker, A., & Lo, M.-H. (2016). A decade of sea level rise slowed by climate-driven hydrology. *Science*, *351*(6274), 699–703.

Reager, J. T., Thomas, B. F., & Famiglietti, J. S. (2014). River basin flood potential inferred using grace gravity observations at several months lead time. *Nature Geoscience*, *7*(8), 588–592.

Richard Peltier, W., Argus, D. F., & Drummond, R. (2018). Comment on “an assessment of the ice-6g_c (vm5a) glacial isostatic adjustment model” by purcell et al. *Journal of Geophysical Research: Solid Earth*, *123*(2), 2019–2028.

Richter, T., Sens-Schönfelder, C., Kind, R., & Asch, G. (2014). Comprehensive observation and modeling of earthquake and temperature-related seismic velocity changes in northern chile with passive image interferometry. *Journal of Geophysical Research: Solid Earth*, *119*(6), 4747–4765.

Rickett, J., & Lumley, D. (2001). Cross-equalization data processing for time-lapse seismic reservoir monitoring: A case study from the gulf of mexico. *Geophysics*, *66*(4), 1015–1025.

Ritzwoller, M. H., Lin, F.-C., & Shen, W. (2011). Ambient noise tomography with a large seismic array. *Comptes Rendus Geoscience*, *343*(8-9), 558–570.

Rodell, M., Chen, J., Kato, H., Famiglietti, J. S., Nigro, J., & Wilson, C. R. (2007). Estimating groundwater storage changes in the mississippi river basin (usa) using grace. *Hydrogeology Journal*, *15*(1), 159–166.

Rodell, M., Famiglietti, J. S., Wiese, D. N., Reager, J., Beaudoing, H. K., Landerer, F. W., & Lo, M.-H. (2018). Emerging trends in global freshwater availability. *Nature*, *557*(7707), 651–659.

Rodell, M., Velicogna, I., & Famiglietti, J. S. (2009). Satellite-based estimates of groundwater depletion in india. *Nature*, *460*(7258), 999–1002.

Rubinstein, J. L., Uchida, N., & Beroza, G. C. (2007). Seismic velocity reductions caused by the 2003 tokachi-oki earthquake. *Journal of Geophysical Research: Solid Earth*, *112*(B5).

Scanlon, B. R., Faunt, C. C., Longuevergne, L., Reedy, R. C., Alley, W. M., McGuire, V. L., & McMahon, P. B. (2012). Groundwater depletion and sustainability of irrigation in the us high plains and central valley. *Proceedings of the national academy of sciences*, *109*(24), 9320–9325.

Sens-Schönfelder, C., & Wegler, U. (2006). Passive image interferometry and seasonal variations of seismic velocities at merapi volcano, indonesia. *Geophysical research letters*, *33*(21).

Shapiro, N. M., Campillo, M., Stehly, L., & Ritzwoller, M. H. (2005). High-resolution surface-wave tomography from ambient seismic noise. *Science*, *307*(5715), 1615–1618.

Silver, P. G., Daley, T. M., Niu, F., & Majer, E. L. (2007). Active source monitoring of cross-well seismic travel time for stress-induced changes. *Bulletin of the Seismological Society of America*, *97*(1B), 281–293.

Simmons, G. (1964). Velocity of shear waves in rocks to 10 kilobars, 1. *Journal of Geophysical Research*, *69*(6), 1123–1130.

Snieder, R. (2006). The theory of coda wave interferometry. *Pure and Applied geophysics*, *163*, 455–473.

Snieder, R., Grêt, A., Douma, H., & Scales, J. (2002). Coda wave interferometry for estimating nonlinear behavior in seismic velocity. *Science*, *295*(5563), 2253–2255.

Sumy, D. F., Neighbors, C. J., Cochran, E. S., & Keranen, K. M. (2017). Low stress drops observed for aftershocks of the 2011 mw 5.7 prague, oklahoma, earthquake. *Journal of Geophysical Research: Solid Earth*, *122*(5), 3813–3834.

Sun, X., & Hartzell, S. (2014). Finite-fault slip model of the 2011 mw 5.6 prague, oklahoma earthquake from regional waveforms. *Geophysical Research Letters*, *41*(12), 4207–4213.

Svoboda, M., LeComte, D., Hayes, M., Heim, R., Gleason, K., Angel, J., … others (2002). The drought monitor. *Bulletin of the American Meteorological Society*, *83*(8), 1181–1190.

Swenson, S., Famiglietti, J., Basara, J., & Wahr, J. (2008). Estimating profile soil moisture and groundwater variations using grace and oklahoma mesonet soil moisture data. *Water Resources Research*, *44*(1).

Syed, T. H., Famiglietti, J. S., Rodell, M., Chen, J., & Wilson, C. R. (2008). Analysis of terrestrial water storage changes from grace and gldas. *Water Resources Research*, *44*(2).

Taira, T., Brenguier, F., & Kong, Q. (2015). Ambient noise-based monitoring of seismic velocity changes associated with the 2014 mw 6.0 south napa earthquake. *Geophysical Research Letters*, *42*(17), 6997–7004.

Taira, T., Nayak, A., Brenguier, F., & Manga, M. (2018). Monitoring reservoir response to earthquakes and fluid extraction, salton sea geothermal field, california. *Science advances*, *4*(1), e1701536.

Tapley, B. D., Bettadpur, S., Ries, J. C., Thompson, P. F., & Watkins, M. M. (2004). Grace measurements of mass variability in the earth system. *science*, *305*(5683), 503–505.

Tapley, B. D., Bettadpur, S., Watkins, M., & Reigber, C. (2004). The gravity recovery and climate experiment: Mission overview and early results. *Geophysical research letters*, *31*(9).

Tian, S., Tregoning, P., Renzullo, L. J., van Dijk, A. I., Walker, J. P., Pauwels, V. R., & Allgeyer, S. (2017). Improved water balance component estimates through joint assimilation of grace water storage and smos soil moisture retrievals. *Water Resources Research*, *53*(3), 1820–1840.

Tsai, V. C. (2011). A model for seasonal changes in gps positions and seismic wave speeds due to thermoelastic and hydrologic variations. *Journal of Geophysical*

Research: Solid Earth, *116*(B4).

Velicogna, I., & Wahr, J. (2006a). Acceleration of greenland ice mass loss in spring 2004. *Nature*, *443*(7109), 329–331.

Velicogna, I., & Wahr, J. (2006b). Measurements of time-variable gravity show mass loss in antarctica. *science*, *311*(5768), 1754–1756.

Wang, H. F. (2017). Theory of linear poroelasticity with applications to geomechanics and hydrogeology. In *Theory of linear poroelasticity with applications to geomechanics and hydrogeology.* Princeton University Press.

Wang, Q., Brenguier, F., Campillo, M., Lecointre, A., Takeda, T., & Aoki, Y. (2017). Seasonal crustal seismic velocity changes throughout japan. *Journal of Geophysical Research: Solid Earth*, *122*(10), 7987-8002.

Wapenaar, K., & Fokkema, J. (2006). Green's function representations for seismic interferometry. *Geophysics*, *71*(4), SI33–SI46.

Watson, K. M., Bock, Y., & Sandwell, D. T. (2002). Satellite interferometric observations of displacements associated with seasonal groundwater in the los angeles basin. *Journal of Geophysical Research: Solid Earth*, *107*(B4), ETG–8.

Wu, W., Zhan, Z., Peng, S., Ni, S., & Callies, J. (2020). Seismic ocean thermometry. *Science*, *369*(6510), 1510–1515.

Wyllie, D. C., & Mah, C. (2004). *Rock slope engineering.* CRC Press.

Wyllie, M., Gardner, G., & Gregory, A. (1962). Studies of elastic wave attenuation in porous media. *Geophysics*, *27*(5), 569–589.

Wyllie, M. R. J., Gregory, A. R., & Gardner, L. W. (1956). Elastic wave velocities in heterogeneous and porous media. *Geophysics*, *21*(1), 41–70.

Yamamura, K., Sano, O., Utada, H., Takei, Y., Nakao, S., & Fukao, Y. (2003). Long-term observation of in situ seismic velocity and attenuation. *Journal of Geophysical Research: Solid Earth*, *108*(B6).

Yao, H., & Van Der Hilst, R. D. (2009). Analysis of ambient noise energy distribution and phase velocity bias in ambient noise tomography, with application to se tibet. *Geophysical Journal International*, *179*(2), 1113–1132.

Yeck, W. L., Hayes, G. P., McNamara, D. E., Rubinstein, J. L., Barnhart, W. D., Earle, P. S., & Benz, H. M. (2017). Oklahoma experiences largest earthquake during ongoing regional wastewater injection hazard mitigation efforts.

Geophysical Research Letters, *44*(2), 711–717.

Young, C. J., Chael, E. P., Zagar, D. A., & Carter, J. A. (1994). Variations in noise and signal levels in a pair of deep boreholes near amarillo, texas. *Bulletin of the Seismological Society of America*, *84*(5), 1593–1607.

Zhai, G., Shirzaei, M., Manga, M., & Chen, X. (2019). Pore-pressure diffusion, enhanced by poroelastic stresses, controls induced seismicity in oklahoma. *Proceedings of the National Academy of Sciences*, *116*(33), 16228–16233.

Zhu, T., Ajo-Franklin, J., Daley, T. M., & Marone, C. (2019). Dynamics of geologic co2 storage and plume motion revealed by seismic coda waves. *Proceedings of the National Academy of Sciences*, *116*(7), 2464–2469.

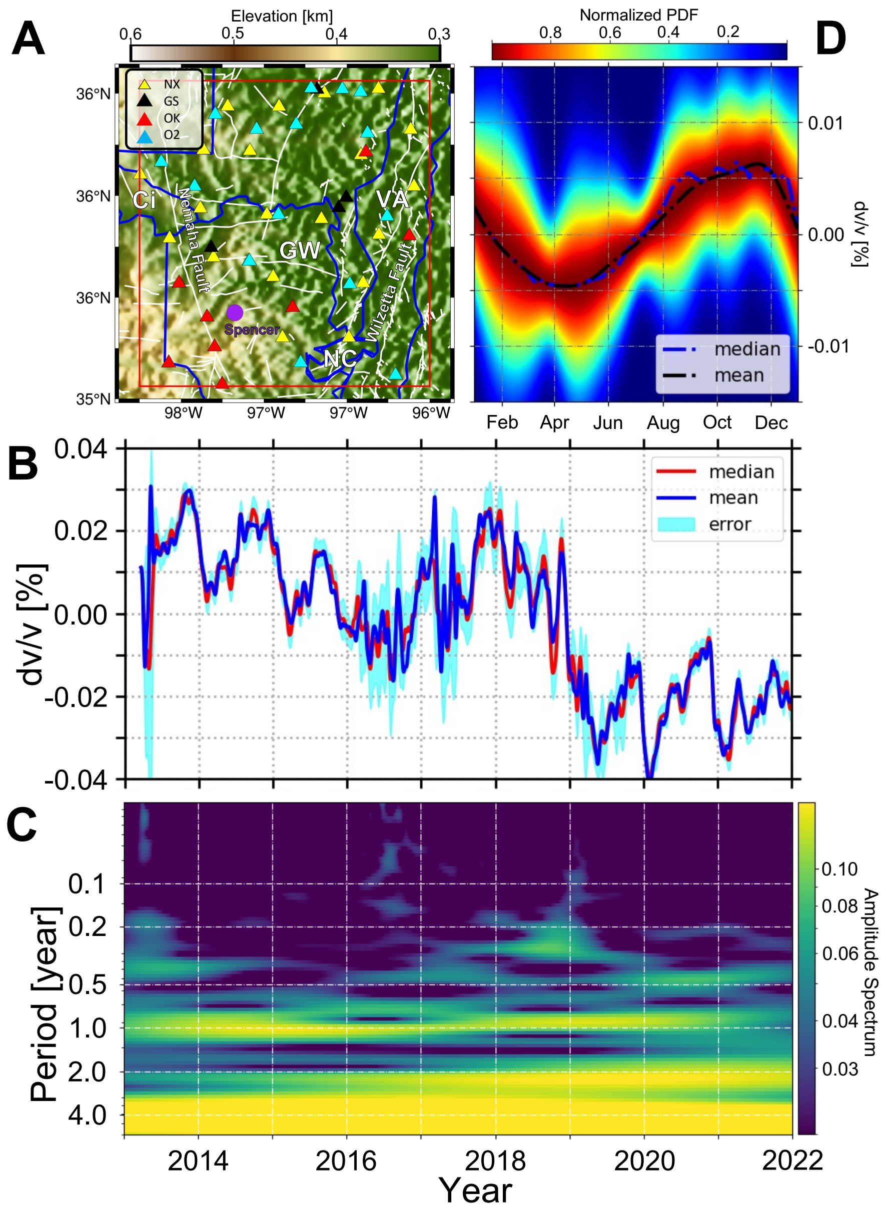

Figure 1. Relative seismic velocity changes measured by ambient noise cross-correlation analysis in central Oklahoma. Available seismometers from different networks are shown as triangles in panel A. Thin white lines denote fault traces mapped at the Earth's surface (Marsh & Holland, 2016), while thick blue lines represent the boundaries of the Garbar-Wellington aquifer (GW), the Vamoosa-Ada aquifer (VA), the North Canadian River (NC), and the Cimarron River (Ci) (`https://www.owrb.ok.gov/maps`). Panel B shows the mean (blue) and median (red) values of the estimated velocity variations, while the blue shades represent the standard error of the measurements. Panel C illustrates the time frequency analysis of the measured dv/v by using short time Fourier analysis. Panel D shows the statistical stacking of the annual pattern of dv/v.

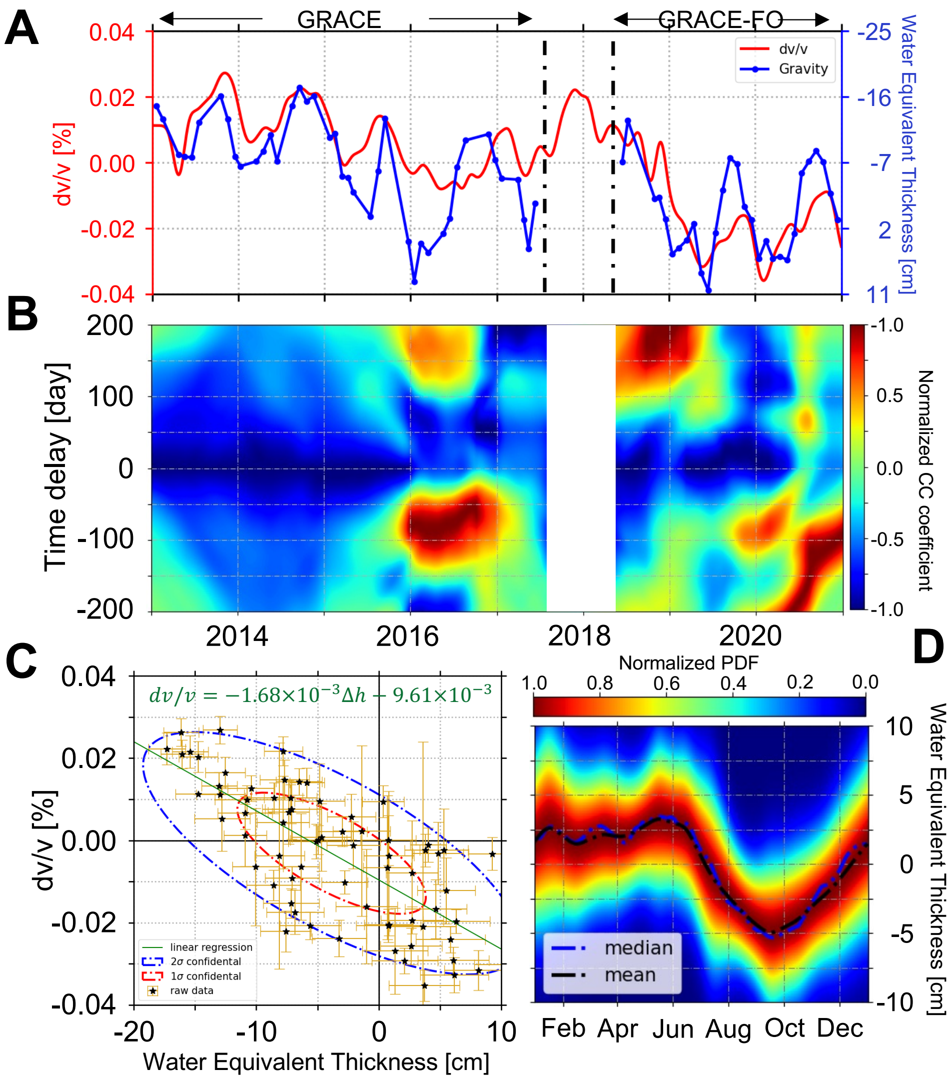

Figure 2. Comparison between relative seismic velocity change (dv/v) with GRACE measurements. Panel A compares dv/v (red) with GRACE measurements (blue) expressed in termes of equivalent water thickness in centimeters. Panel B illustrates the local cross-correlation map between dv/v and GRACE observations. The gap in Panels A and B comes from the survey gap between GRACE and GRACE-FO missions. Panel C shows the relation between dv/v and GRACE results (h) through a linear regression. Yellow bars represent the standard errors of dv/v and GRACE measurements. Panel D shows the statistical stacking of the annual pattern of the GRACE measurements.

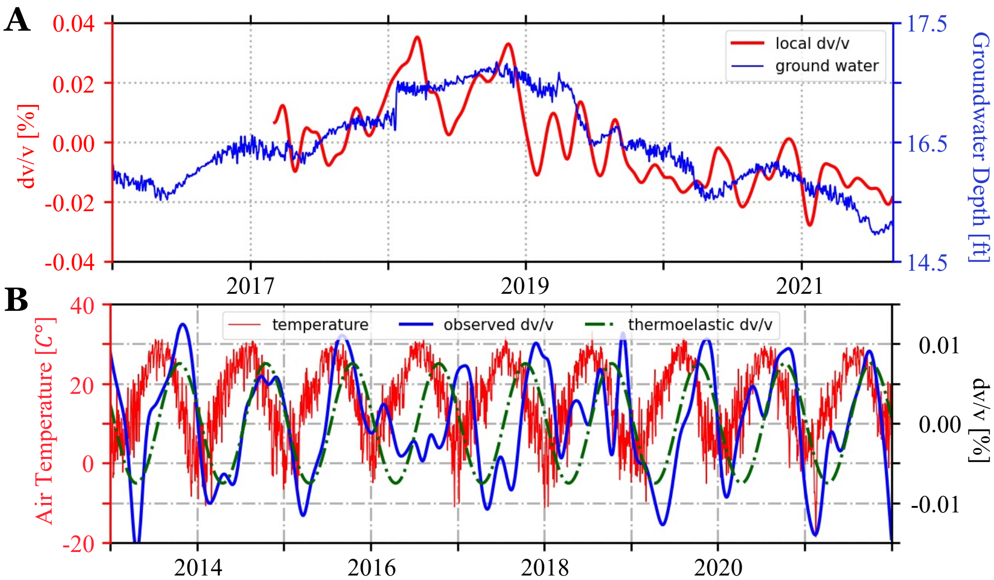

C

Thermo-elastic modeling parameters

Parameter	Value	Reference
Linear thermo-expansion α_{th}	$1 \times 10^{-5}\ °C^{-1}$	Tsai (2011)
Reference wavenumber k	$2\pi/(40\mathrm{km})$	Mordret et al. (2016)
Thermo-diffusivity κ	$6.43 \times 10^{-7} m^2/s$	Deming and Borel (1995)
First Lamé constant λ	$81 GPa$	Ji et al. (2010)
Poisson ratio ν	0.386	Wyllie and Mah (2004)
Second Lamé constant μ	$24 GPa$	Wyllie and Mah (2004)
Mean temperature T_0	$15.79\ °C$	Temperature History
Frequency ω	$2 \times 10^{-7} s^{-1}$	Temperature History
Incompetent layer thickness y_b	$2.899 m$	Grid Search
Murnaghan constant m	$-1.78 \times 10^7 GPa$	Grid Search

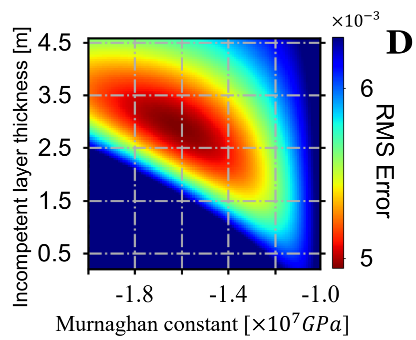

Figure 3. Analysis of potential causes of long-term and seasonal cycling of measured seismic velocity variations. The black line in panel A represents the historical measurement of groundwater depths for the Spencer well (purple dot in Figure 1A), while the red line is the local dv/v computed from three seismometers in the vicinity of the well (OK.CHOK, OK.SMO, OK.SWND). Panel B compares simulated velocity variations (green dashed line) from a thermo-elastic modeling (Ben-Zion & Leary, 1986; Tsai, 2011) with the historical air temperature (red) recorded in central Oklahoma. Panel C gives model parameters used in the thermo-elastic calculation, in which the incompetent layer thickness y_b and the Murnaghan constant m are determined by a grid search shown in panel D.

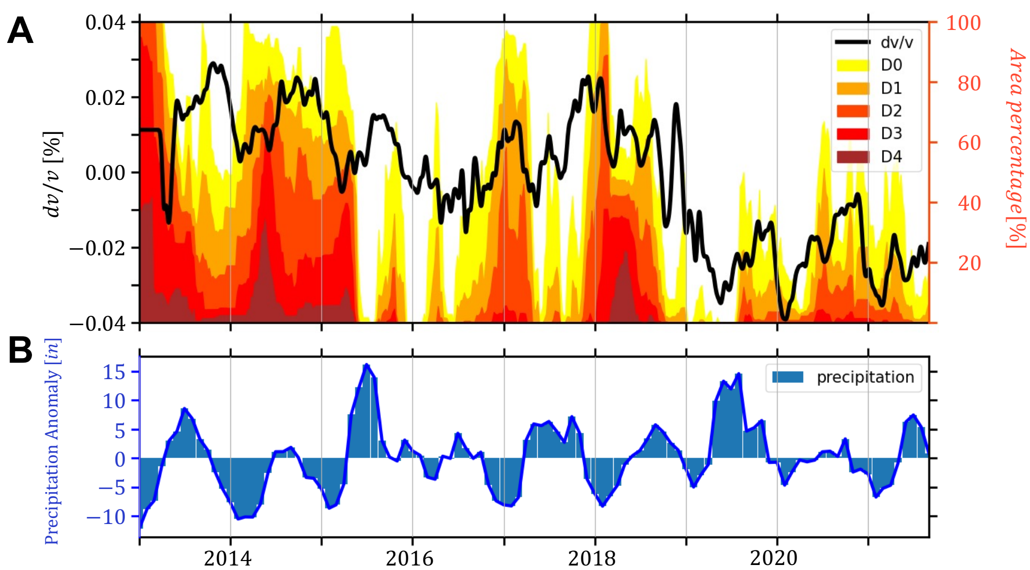

Figure 4. Comparison among dv/v, drought index and precipitation records in central Oklahoma. Panel A compares measured dv/v (black) with drought index from the U.S. Drought Monitor, expressed as the area percentage under different drought categories (`droughtmonitor.unl.edu`). The severity of drought increases from D0 to D4. Panel B presents the precipitation records in central Oklahoma, collected from the Oklahoma Climatological Survey (`http://climate.ok.gov`).

Supporting Information for "Monitoring terrestrial water storage, drought and seasonal changes in central Oklahoma with ambient seismic noise"

Shuo Zhang[1], Bingxu Luo[1], Yehuda Ben-Zion[2], David E. Lumley[1,3], Hejun Zhu[1,3]

[1]Department of Geosciences, the University of Texas at Dallas

[2]Department of Earth Science, University of Southern California

[3]Department of Physics, the University of Texas at Dallas

Contents of this file

Text S1 to S4

Figure S1 to S8

Introduction

In this supporting document, we provide additional details on data processing and analysis to support discussions in the main text. Section S1 illustrates the dominant frequency ranges of raw data and the corresponding depth sensitivity kernels; Section S2 shows the decomposition of dv/v into long-term trends, seasonal cycling, and short-term perturbations; Section S3 examines the uncertainty of dv/v with respect to different azimuthal angles and frequency ranges; Section S4 compares observed dv/v with simulated soil moisture near the Earth's surface in Oklahoma.

Text S1. Frequency spectrum and depth sensitivity kernels

Investigating the probability power density function of raw data, we find the dominant frequencies of ambient noise in central Oklahoma range from 1 to 100s (Figure S1), which are similar to the general survey in North America (McNamara & Buland, 2004). Considering the depth sensitivity kernels of fundamental mode Rayleigh wave (Figure S2), we filter the raw data from 1 to 10s in order to investigate groundwater distribution at depths shallower than $1 - 2km$.

Text S2. Postprocessing of dv/v

The time series of dv/v can be decomposed into three components: long-term trend, seasonal cycling, and short-term perturbations (Figure S4). Applying a Gaussian filter, the high-frequency perturbations are removed from the raw dv/v. Based on the least-square regression, the long-term trend of dv/v can be expressed by a 20th-order polynomial. Finally, the seasonal cycling of the dv/v is the subtraction of the long-term trend from the smoothed dv/v.

Text S3. Uncertainty of dv/v

Daily CCFs have different behaviors within different frequency ranges (Figure S5). Except for 0.1-1.0 Hz, we filter the raw data with different frequency bands (0.5-2.0 Hz, 0.2-0.8 Hz, 0.4-1.6 Hz) and then to compute dv/v (Figure S6). In spite of local disagreements, the similarity among time series with different frequency bands suggests acceptable uncertainties of our measurements.

Although we assume a homogeneous velocity perturbation, the changes in ambient noise cross-correlation functions could also be generated by heterogeneous noise source distributions, such as periodic ocean tides (Ardhuin et al., 2011) and wind speeds (Young et al., 1994). Hence, we re-group the station pairs based on different azimuthal directions, i.e., 0 to 90°, 90 to 180°, 180 to 270°, 270 to 360°, respectively, in order to evaluate the changes of dv/v with respect to azimuthal angles (Figure S7). The similar patterns of long-term and seasonal cycling among these four groups suggest that our measured changes mainly result from subsurface velocity changes in Oklahoma, rather than the consequence of noise source variations.

Text S4. Soil Moisture Simulation

In order to further understand the seasonal cycling pattern, we also compare dv/v with modeled soil moisture storage (SMS) in central Oklahoma, collected from the North American Land Data Assimilation System (NLDAS-LSM) (Cosgrove et al., 2003; Mitchell et al., 2004). The spatial resolution of the SMS models is 0.125° in longitude and latitude, and their temporal sampling is one month. Three LSMs models (NOAH, MOSAIC, and VIC) are the simulations of water balance near the Earth's surface based on the accumulation of precipitation, surface/subsurface runoff, evapotranspiration, etc (Rui & Mocko, 2022). The MOSAIC model accounts for subgrid vegetation variability with a tile approach. Each tile has a predominant soil type and three discontinuities at $10cm$, $40cm$, and $200cm$ depths respectively. The first two layers are in the root zone. In the NOAH model, four soil layers are set with thicknesses of $10cm$, $30cm$, $60cm$, and $100cm$. The first three layers are from the root zone in non-forested region with the fourth in forested regions. The thicknesses of three layers in the VIC model are spatially variable. Therefore, the root zone in the model is determined by local vegetation types. The first two layers contain the energy-balanced snow model.

Since the NLDAS-LSM models give us results at different depths, in this study, we extract their temporal evolutions at depths ranging from 0 to 100 cm (Figure S8A). All SMS models show inter-annual cycling, which matches our dv/v measurements. Taking the NOAH model as an example, we also check its behavior at different depths (Figure S8B). Results from all depths have a similar intra-annual pattern with dv/v observations.

Other than groundwater storage, these comparisons suggest the sensitivity of dv/v with respect to soil moisture, especially for the inter-annual trend. However, these SMS simulations can only predict the distribution of soil moisture within hundreds of centimeters, while surface and coda waves used in this study might not sensitive to such shallow parts of the crust (Figure S2). More investigations are needed to better clarify the impact of soil moisture on near-surface seismic velocity.

References

Ardhuin, F., Stutzmann, E., Schimmel, M., & Mangeney, A. (2011). Ocean wave sources of seismic noise. *Journal of Geophysical Research: Oceans*, *116*(C9).

Cosgrove, B. A., Lohmann, D., Mitchell, K. E., Houser, P. R., Wood, E. F., Schaake, J. C., … others (2003). Real-time and retrospective forcing in the north american land data assimilation system (nldas) project. *Journal of Geophysical Research: Atmospheres*, *108*(D22).

McNamara, D. E., & Buland, R. P. (2004). Ambient noise levels in the continental united states. *Bulletin of the seismological society of America*, *94*(4), 1517–1527.

Mitchell, K. E., Lohmann, D., Houser, P. R., Wood, E. F., Schaake, J. C., Robock, A., ... others (2004). The multi-institution north american land data assimilation system (nldas): Utilizing multiple gcip products and partners in a continental distributed hydrological modeling system. *Journal of Geophysical Research: Atmospheres*, *109*(D7).

Rui, H., & Mocko, D. (2022, 7). Document for north american land data assimilation system phase 2 datasets (nldas-2.0 in netcdf format) [Computer software manual]. Greenbelt, MD 20771 USA.

Young, C. J., Chael, E. P., Zagar, D. A., & Carter, J. A. (1994). Variations in noise and signal levels in a pair of deep boreholes near amarillo, texas. *Bulletin of the Seismological Society of America*, *84*(5), 1593–1607.

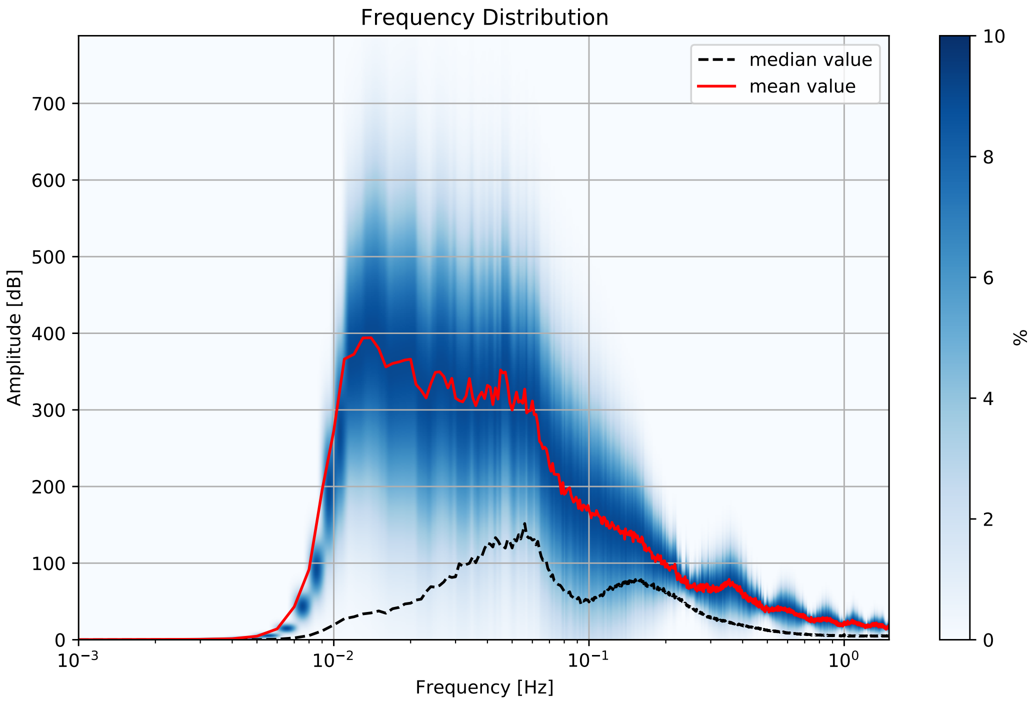

Figure S1. Probability distribution function (PDF) of the frequency spectra of all available seismic recordings in this study. The dominant period of ambient seismic noise ranges from 1 to 100s in central Oklahoma. Regarding the penetrating depths of surface waves, we filter the raw data into 1 to 10s.

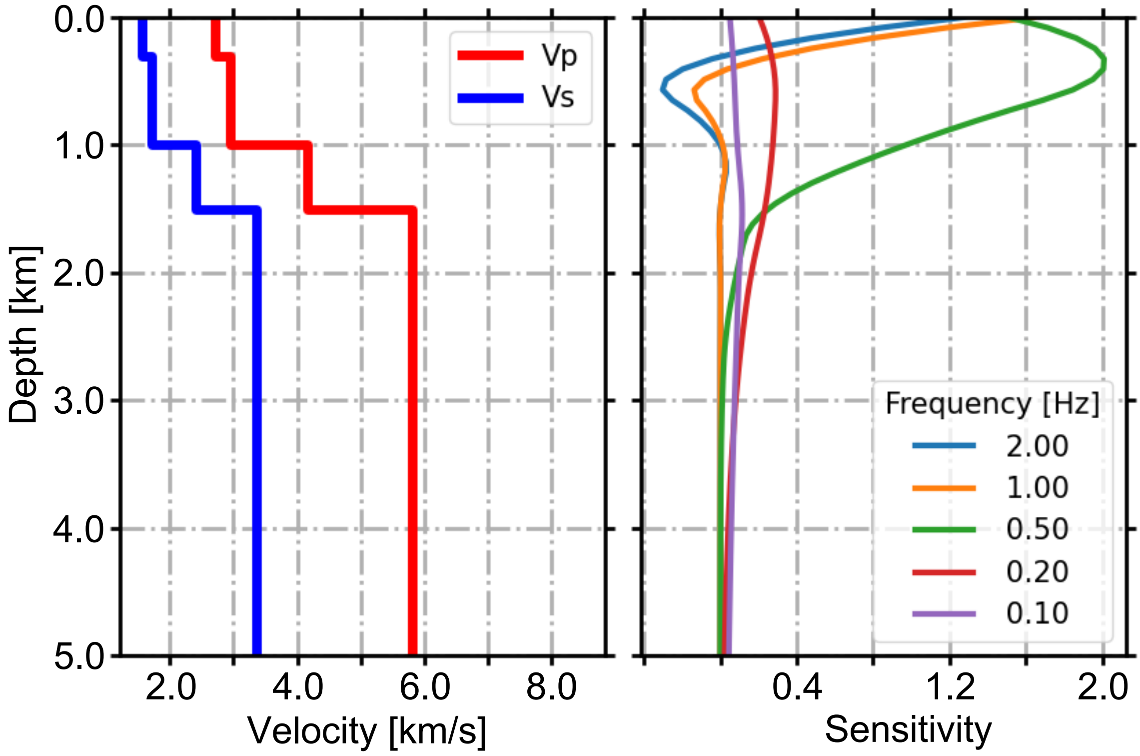

Figure S2. Depth sensitivity kernels of fundamental mode Rayleigh wave (right) based on the 1-D velocity model (left) provided by the Oklahoma Geological Survey. The Vp/Vs ratio is set as 1.732.

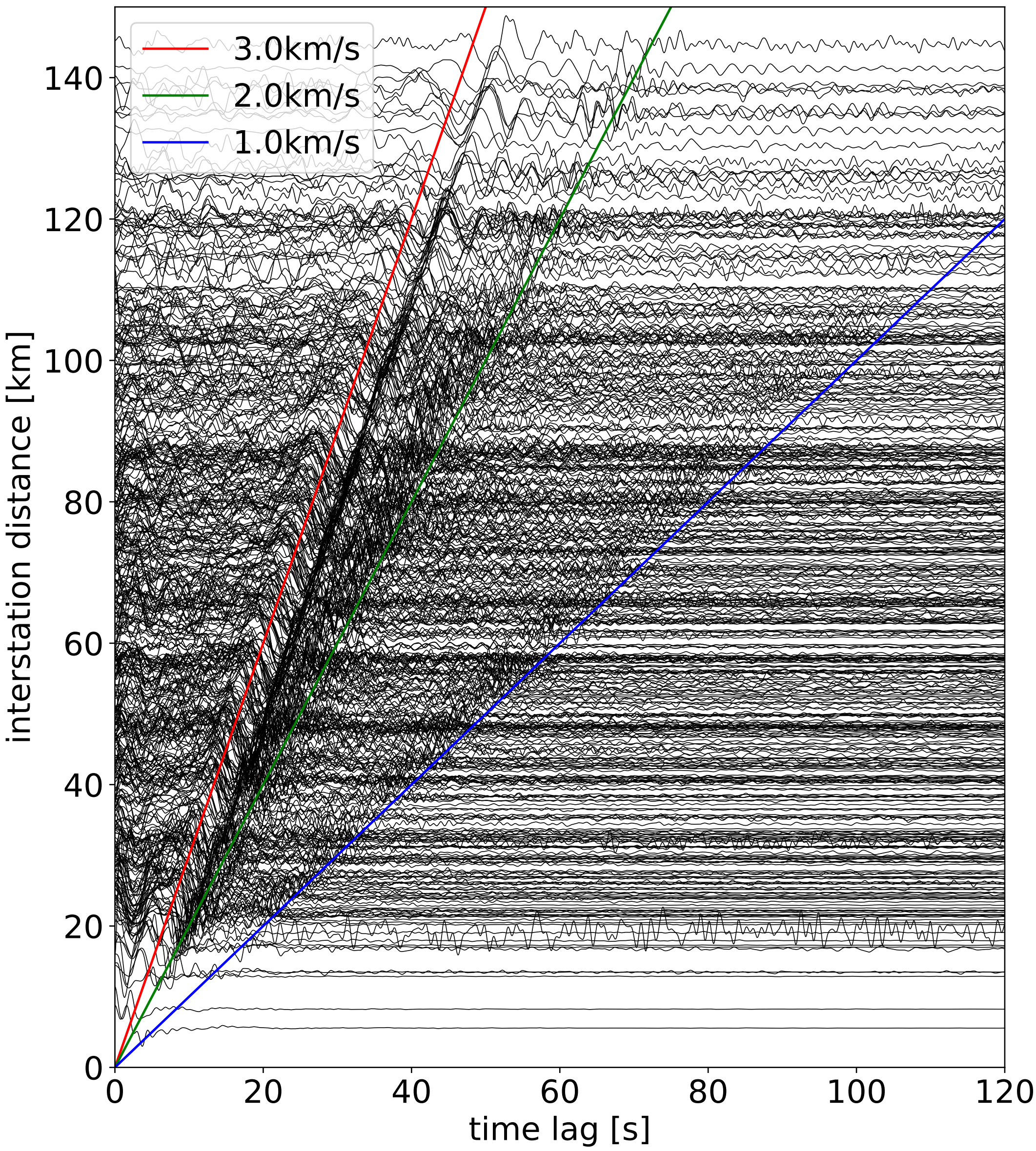

Figure S3. Reference cross-correlation functions of all station pairs, aligned as the function of inter-station distance. Contributions from surface and coda waves can be isolated by apparent velocities, $3.0km/s$ and $2.0km/s$, respectively

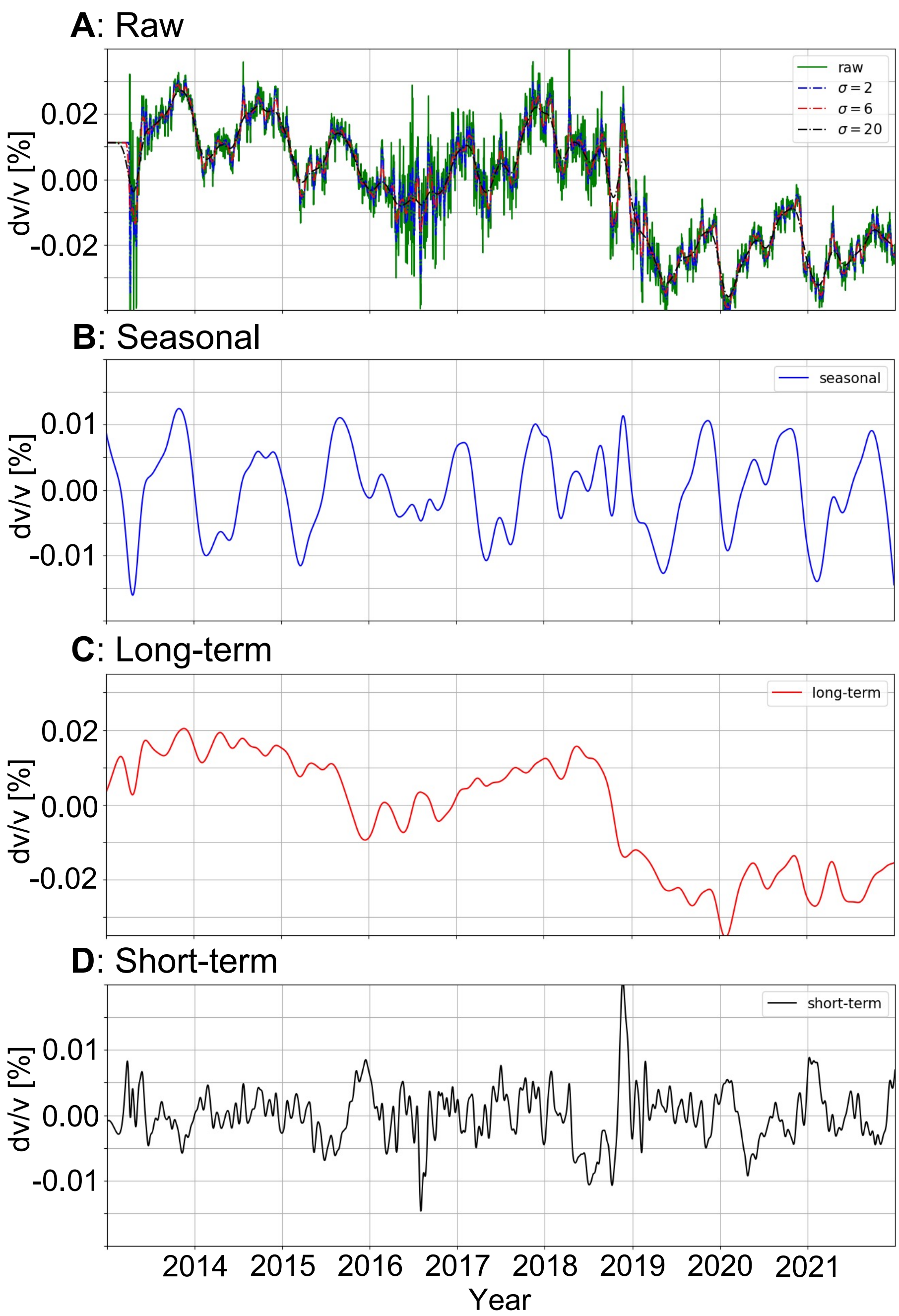

Figure S4. Decomposition of raw dv/v in central Oklahoma. The long-term trend (C) is fitted by a 20th-order polynomial by a least-square regression. Seasonal cycling (B) is the subtraction of the long-term trend (C) from the smoothed dv/v (A). Removing both long-term trends and seasonal cycling, the residual dv/v represents short-term perturbations (D).

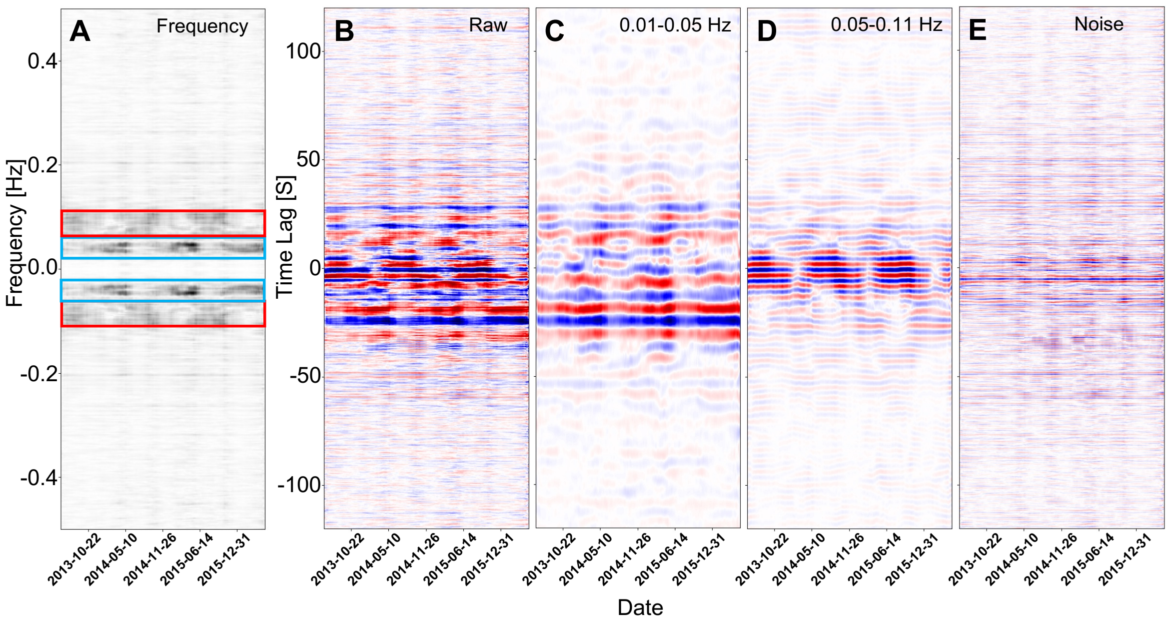

Figure S5. Taking station pair NX.STN03 and NX.STN32 as an example, different frequency ranges in daily cross-correlations give us different patterns.

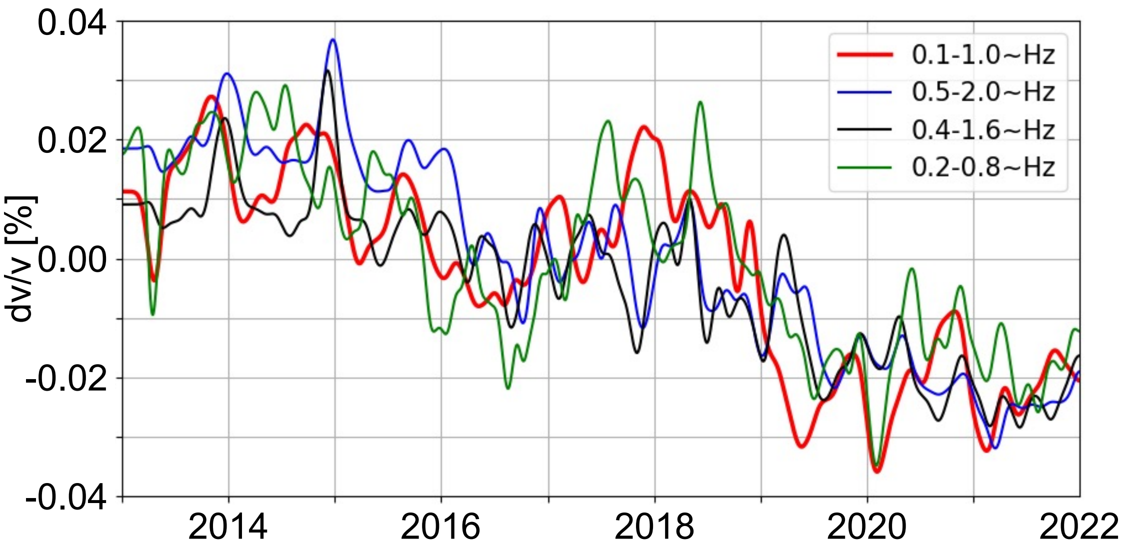

Figure S6. The similarity of dv/v with different frequency bands suggests acceptable uncertainty of seismic velocity with respect to the frequency band. As a comparison, the thick red line is the one used in the main text for discussion.

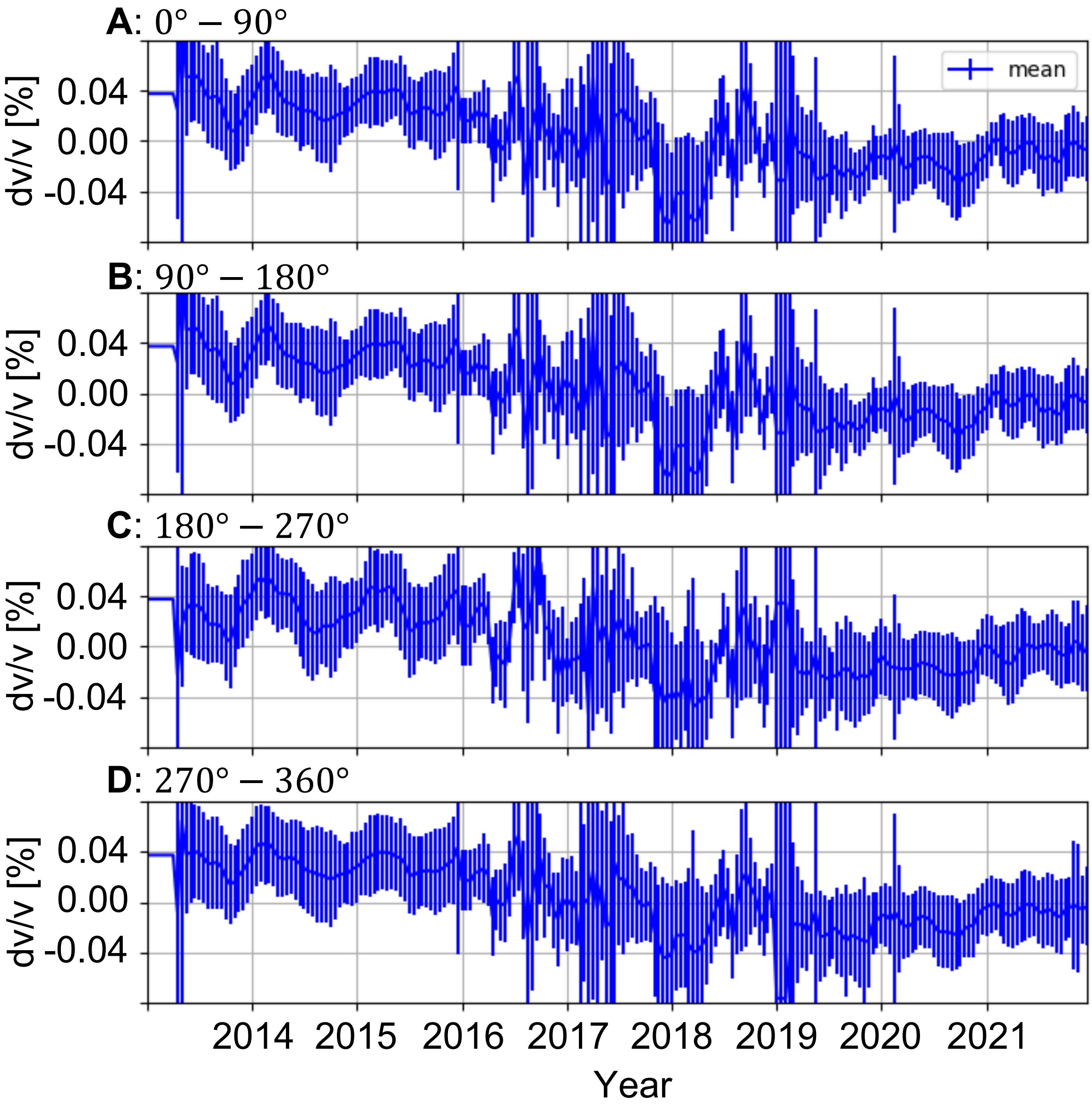

Figure S7. Uncertainty of dv/v with respect to different azimuthal angles. From top to bottom are the results with azimuthal angles of 0-90°, 90-180°, 180-270°, and 270-360°, respectively. Different azimuthal angles give us dv/v measurements with similar seasonal cycling and long-term trend.

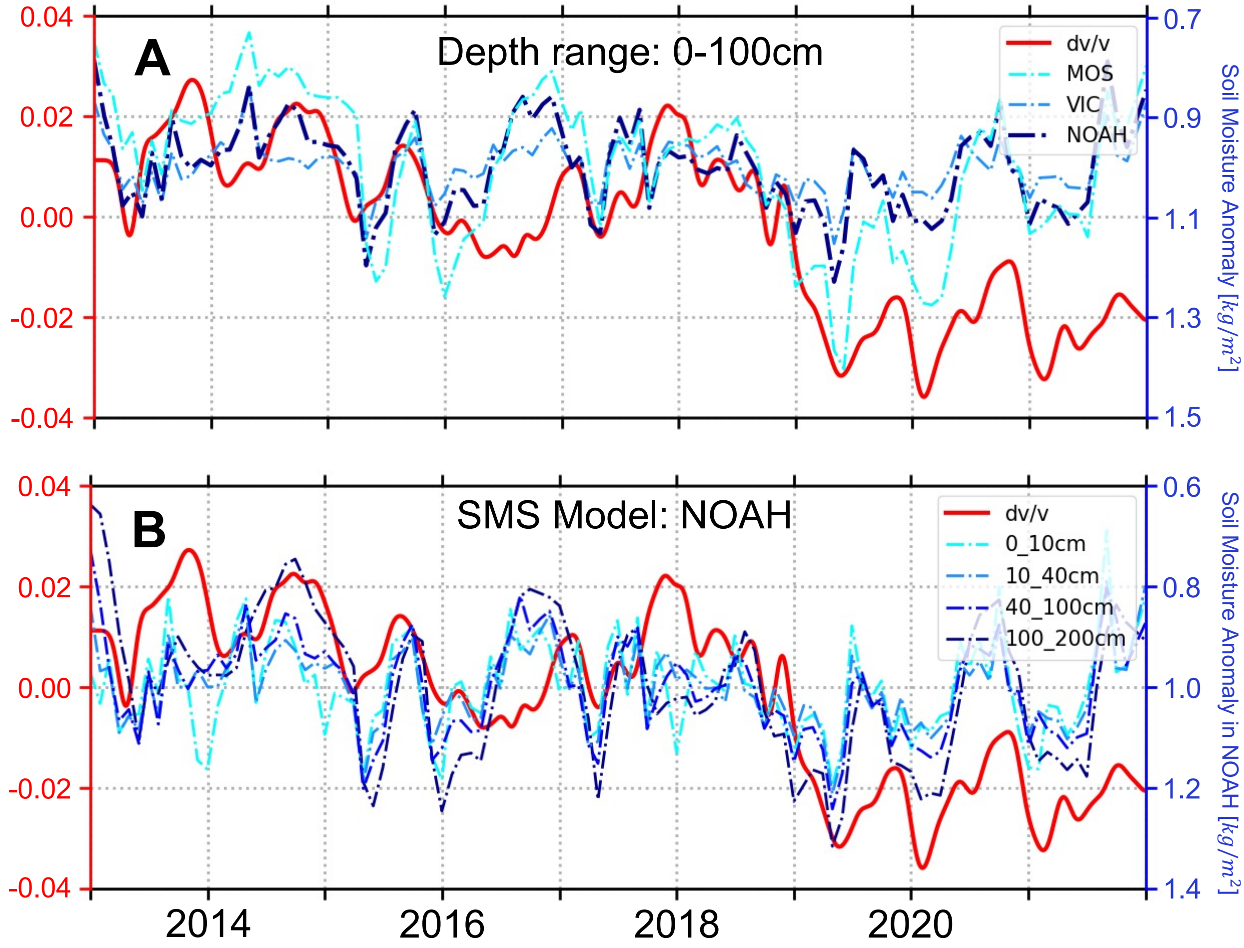

Figure S8. Comparison among dv/v and soil moisture simulations from different models. Panel A shows soil moisture simulations at 100cm depth from MOSAIC, VIC, and NOAH models. Panel B illustrates the results from model NOAH at different depths. All soil moisture simulations, with different depths and model settings, are consistent with the measured intra-annual cycling of dv/v.